Turkish Journal of Physics

http://journals.tubitak.gov.tr/physics/

Research Article

Turk J Phys
(2018) 42: 166 – 174
© TÜBİTAK
doi:10.3906/fiz-1708-1

Spectral properties of the galactic supernova remnant Vela Jr. (G266.2–1.2) using *Chandra*

Nergis CESUR[1,*], **Aytap SEZER**[2], **Murat HÜDAVERDİ**[1]
[1]Department of Physics, Faculty of Arts and Science, Yıldız Technical University, İstanbul, Turkey
[2]Department of Electrical-Electronics Engineering, Faculty of Engineering and Architecture, Avrasya University, Trabzon, Turkey

Received: 02.08.2017 • **Accepted/Published Online:** 25.09.2017 • **Final Version:** 26.04.2018

Abstract: An X-ray nonthermal spectral investigation of the galactic shell-type supernova remnant (SNR) Vela Jr. using archival data from *Chandra* for the northern and northwestern rims of the SNR is presented. Spectra were extracted from four emission regions in these rims (three in the northwestern rim and one in the northern). The X-ray spectra of the northwestern rim were well reproduced by a single *power-law* and the synchrotron model *srcut*, and for the north rim, the spectra were fitted by a single and a *broken power-law*, respectively. The spectra of both rims show no line emission. Each spectrum was fit by subtracting the modeled and nonmodeled background spectra, and statistically acceptable fits to all regions were derived using each model. Slight variations in derived fit parameters (such as photon index and roll-off frequency) with the background modeling method are also reported.

Key words: X-rays, interstellar medium, supernova remnants, Vela Jr., (G266.6–1.2, RX J0852.0–4622)

1. Introduction

Shocks of supernova remnants (SNRs) are known as cosmic ray accelerators. They are widely believed to be the primary sites for the galactic cosmic ray acceleration mechanism up to the "knee" of the cosmic ray spectrum at energies of approximately 10^3 TeV. As revealed by the X-ray observatories, shells of several young SNRs are synchrotron X-ray emitters and particle accelerators [1,2]. Considering that, synchrotron X-ray from SNRs is a powerful tool to understand the cosmic ray acceleration processes. However, observations of the SNRs with synchrotron X-ray emitting shells are limited [3]. The first observational result of the synchrotron X-rays was from shells of SN 1006 [1] and indicated that SNRs accelerate electrons up to approximately TeV energies. Recently, nonthermal X-ray emission has been detected from a growing number of SNRs in the galaxy with modern X-ray observatories (e.g., G347.3–0.5 [2,4]; G266.2–1.2 [5]; G111.7-02.1 [6]). Young SNR Vela Jr. (also called RX J0852.0–4622 and G266.6–1.2) was originally discovered in the *ROSAT* All-Sky Survey data [7]. Vela Jr. is a nearby and young SNR, circular with a diameter of approximately 2° in the line of sight to Vela SNR. The age and the distance of Vela Jr. were estimated as 2400–5100 years and 0.5–1 kpc [8], respectively. It has a synchrotron X-ray shell [5,9] and is one of the few TeV-emitting SNRs. Its emission is particularly enhanced along limbs (e.g., northern (N), northwestern (NW), southern). The NW rim was reported to have bright synchrotron X-ray filaments [9]. With the *ROSAT* data, the nonthermal emission of the SNR was reported to have a photon index (Γ) of approximately 2.6 [7]. Also, in the *ASCA* study, X-ray emission from bright rims

*Correspondence: nergis.cesur.507@std.yildiz.edu.tr

of the SNR was to be characterized by a power-law with a Γ of approximately 2.6 [5]. In the *Chandra* spectral analysis of the NW rim of the SNR, the photon index was approximately 2.7 [9], while in the *XMM-Newton* analysis it was approximately 2.6 [10].

In recent years, the importance of background modeling in spectral analysis has been emphasized in many studies (e.g., [11–13]). It is a key process to understand the effect of the SNR's environment (e.g., its distance from the galactic latitude) on its X-ray emission spectrum.

Analyzing nonthermal emission in the SNRs with various nonthermal models provides information about the key spectral properties of the emission (such as photon index and roll-off frequency). By using these results, several features about the remnant might be extracted.

Maximum energy of accelerated electrons ($E_{max,e}$) and the magnetic field strength (B) determine the spectrum of synchrotron emission, which is a roll-off energy and a key observational feature [14]. In other words, these parameters are constrained by measuring the roll-off frequency of the spectrum (ν_{roll}), which is proportional to $BE^2_{max,e}$ and corresponds to the characteristic synchrotron frequency of electrons with $E_{max,e}$ [15], [16]. Also, synchrotron X-rays indicate that young SNRs act as electron accelerators up to 10–100 TeV [1], and they are emitted by electrons whose energy is near $E_{max,e}$ [9,17,18]. As they age, the roll-off frequency becomes smaller [3].

Therefore, precise background modeling is critical in estimating the reliable values of roll-off frequency and other spectral parameters, no matter what model is used (thermal or nonthermal).

In this paper, the X-ray spectral properties of the NW and N rims of Vela Jr. are investigated based on approximately 39, 35, and 40 ks *Chandra* observations. For this investigation, the *Chandra* data of the NW and N rims of the SNR were reanalyzed. Two background estimation techniques were applied for each spectrum of Vela Jr., subtracting the nonmodeled (BGD-1) and modeled background (BGD-2) spectra to emphasize the background estimation technique by taking the galactic location of the SNR into consideration for a comparable study with three *Chandra* observations. The background regions were extracted from the same field of view for each observation (dashed areas in Figures 1 and 2).

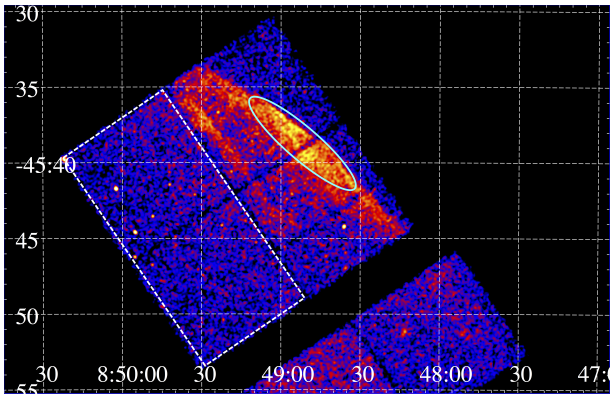


Figure 1. *Chandra* ACIS-I image of the N rim of Vela Jr. in the 2–7 keV energy band. The spectral analysis region is shown by the cyan elliptical area. The dashed lined rectangular region represents the background region.

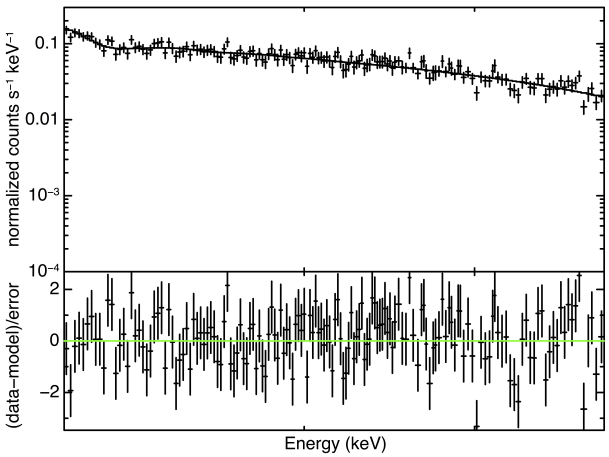


Figure 2. BGD-2 subtracted spectrum of the selected emission region on the N rim of the SNR, fitted with an absorbed *power-law* model in the 2–5 keV energy band.

This paper is organized as follows. In Section 2, the *Chandra* observations and the data reduction techniques are described and the spectral analysis procedures are presented. The results are discussed in Section 3. The conclusions are summarized in Section 4.

2. Analysis

2.1. X-ray observations and data reduction

Archival data acquired by *Chandra* were analyzed as summarized in Table 1. The fields of view are shown in Figures 1 and 2. The observations were performed by Advantage CCD Imaging Spectrometer (ACIS-I and ACIS-S). In the analysis, the most recent data reduction algorithms and calibration products were used (Heasoft 6.20 (https://heasarc.nasa.gov/lheasoft/), CIAO 4.8 (http://cxc.harvard.edu/ciao/), CALDB 4.7.0, XSPEC 12.9.1 (https://heasarc.gsfc.nasa.gov/xanadu/xspec/), and AtomDB 3.0.8 [19,20]). As in the standard procedure by the Chandra X-Ray Center (http://cxc.harvard.edu/index.html), the event list *Chandra* files were reprocessed using the script *chandra_repro*, and the *dmcopy* script was used on the event files for restricting the energy ranges and creating the images. In order to improve the statistics of the models and to present the characterization of spectra clearly, the spectrum files of the NW rim observations were merged (Obs. Id. 3846 and Obs. Id. 4414). Hence, the *combine_spectra* task was used in CIAO to combine each spectrum file.

Table 1. *Chandra* observations of the N and NW rims.

Rims of Vela Jr.	Obs. Id.	Dates	Pointing directions (α_{J2000}, δ_{J2000}) (α_{J2000}, δ_{J2000})	Detectors	Exp. (ks)
NW	3846	2003-08-31	$08^h49^m07^s.92$, –45°37′44.40	ACIS-S	39
NW	4414	2003-01-06	$08^h49^m07^s.92$, –45°37′44.40	ACIS-S	35
N	9123	2008-08-31	$08^h49^m18^s.00$, –45°42′46.00	ACIS-I	40

2.2. X-ray spectral analysis

Figures 1 and 2 show ACIS-I and ACIS-S images of the N and NW rims of Vela Jr. in the 2.0–7.0 keV energy band. The emissions of specific regions were characterized. For the NW rim of the SNR, two elliptical regions centered at the source location with areas of 2.59 and 1.71 arcmin^2 were selected, and a third source was selected excluding these regions from it, with an area of 14.65 arcmin^2. For the N rim of the SNR, the emission was selected from a 15.22 arcmin^2 elliptical area. All these regions are shown by solid ellipses in Figures 1 and 2, respectively, and they were selected through their X-ray peak emissions.

For the *Chandra* observation of the N rim of the SNR, the background spectrum was extracted from a source-free region in the same field of view (the white dashed rectangular area in Figure 1).

For the *Chandra* observation of the NW rim of Vela Jr., because of the difference of background levels among the back-illuminated chips and the front-illuminated chips in the ACIS-S detector, the background spectrum was extracted from a source-free area in the same chip, near the selected regions (the magenta dashed rectangular area in Figure 2).

2.2.1. Background estimation

For both the N and NW rims of Vela Jr., the spectra of the selected sources were first fitted by subtracting the BGD-1. Next, the background spectra of the sources on the NW and N observations were modeled with a specific approach (BGD-2).

Vela Jr. is on the galactic plane (l = 266.°259, b = –01.°220), so possible contamination of the galactic ridge X-ray emission (GRXE) was evaluated [21]. First, the background spectrum of the N rim was fit with GRXE, in addition to the fixed cosmic X-ray background (CXB) model [22]. For the GRXE model, a photo-absorbed two-temperature thermal plasma emission model (*apec* in XSPEC) was employed. Electron temperature (kT_e) parameters were set for high- and low-temperature plasma-free, and the absorption column density provided by [23] was assumed for the remnant, as in [24]. Also, these parameters were fixed to the galactic column density $N_H = 4.0 \times 10^{22}$ cm^{-2} with plasma temperatures of 1.66 keV and 15.1 keV [24,25]. Both models yielded statistically unacceptable fits (χ^2/degrees of freedom (d.o.f.) > 2) and very high kT_e values, which are not physically meaningful.

Next, GRXE emission was neglected by assuming its affectless feature on the spectra. Hence, for the N rim, the background spectrum was fit properly with the assumption that the emission contains CXB and foreground emission (FE). The background spectrum was fitted with a model of *Abs1* × *power-law* + *apec*, where *apec* is a collisional ionization equilibrium plasma model in the XSPEC and represents the FE component, while an absorbed *power-law* model represents the CXB emission defined under the assumption of a power-law shape with a photon index of 1.41 and a surface brightness value of 5.41×10^{-15} erg s^{-1} cm^{-2} arcmin^{-2} in the 2–10 keV band [22]. Next, the background spectrum was simulated using the *fakeit* command in XSPEC and subtracted from the source spectrum. All spectra were grouped with 25 counts bin^{-1}. The best-fit parameters of the background spectrum are shown in Table 2.

Table 2. Best-fit parameters for the background spectrum of the northern rim of Vela Jr. (hereafter, parentheses indicate single-parameter 90% confidence intervals).

Component	Parameter	Values
CXB (*power-law*)	N_H (10^{22} cm^{-2})	0.67 (fixed)
	Photon index	1.41 (fixed)
	S.B. (erg s^{-1} cm^{-2} arcmin^{-2})*	5.41×10^{-15} (fixed)
FE (*apec*)	kT (keV)	0.671 (0.717–0.762)
	norm (10^{-3} photons cm^{-2} s^{-1})	0.744 (0.866–1.106)
	χ^2/ d.o.f.	290.64 / 340

*Surface brightness in the 2–10 keV band [22].

As in the background modeling for the N rim observation, the GRXE component was negligible. Hence, fitting the background spectrum with a single CXB component was sufficient for the spectral analysis for this region. The aforementioned parameters were used for the CXB component, except that the column density was set free. Same as the previous background modeling, the background spectrum was simulated using the *fakeit* command and subtracted from the source spectrum. All spectra were grouped with 25 counts bin^{-1}. The best-fit parameters of the background spectrum for the NW rim are shown in Table 3.

Table 3. Best-fit parameters for the background spectrum of the NW rim of Vela Jr.

Component	Parameter	Values
CXB (*power-law*)	N_H (10^{22} cm^{-2})	2.51 (3.29–1.83)
	Photon index	1.41 (fixed)
	S.B. (erg s^{-1} cm^{-2} arcmin^{-2})*	5.41×10^{-15} (fixed)
	χ^2/ d.o.f.	262.44 / 341

*Surface brightness in the 2–10 keV band [22].

2.2.2. Spectral fitting

The absorption column density was fixed at 6.7 $\times$ 10^{21} cm^{-2} [26] (*tbabs* in XSPEC [27]), with the metal abundance adopted from [27]. An energy range of below 2 keV was restricted to avoid thermal contamination from the Vela SNR for all fits because of ambiguity caused by this remnant [26].

The spectral analysis region on the N rim was fitted with an absorbed *single power-law* model in XSPEC. Then the same region was fitted with the BGD-2 subtracted spectrum with an absorbed single *power-law* and an absorbed *broken power-law* model, respectively. The absorbed *broken power-law* model gave an acceptable reduced chi-square value compared with the absorbed single *power-law* model. In all fits, N_H was always fixed to 6.7 $\times$ 10^{21} cm^{-2}, as mentioned before, and Γ, breaking energy, and the normalizations were set as free parameters. All spectra were fitted in the 2.0–5.0 keV effective energy band. The best-fit parameters are shown in Tables 4 and 5 for BGD-1 and BGD-2 spectra, respectively. The BGD-2 subtracted ACIS-I spectrum is shown in Figure 3.

Table 4. Best-fit parameters for BGD-1 subtracted spectrum of selected emission region in the N rim of Vela Jr.

Component	Parameter	Values
power-law	N_H (10^{22} cm^{-2})	0.67 (fixed)
	Photon index	2.55 (2.63–2.47)
	norm (10^{-3} photons cm^{-2} s^{-1})	3.02 (3.32–2.75)
	χ^2/ d.o.f.	208.46 / 195

Table 5. Best-fit parameters for the BGD-2 spectrum of the selected emission region on the N rim of Vela Jr.

Component	Parameter	Values
broken power-law	N_H (10^{22} cm^{-2})	0.67 (fixed)
	Photon Index1	2.37 (2.45–2.29)
	Photon Index2	0.15 (0.65–(-0.37))
	Breaking energy (keV)	2.0 (fixed)
	norm (10^{-3} photons cm^{-2} s^{-1})	2.93 (3.21–2.68)
	χ^2/ d.o.f.	196.59 / 193

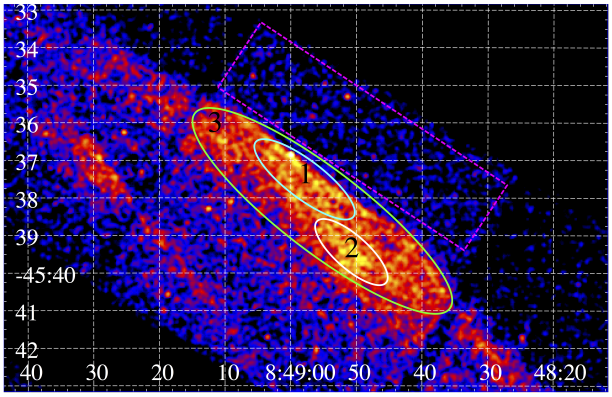


Figure 3. *Chandra* ACIS-S image of the NW rim of Vela Jr. in the 2–7 keV energy band. The spectral analysis regions are shown by cyan (1), white (2), and green (3) elliptical areas. The background region is shown by the magenta dashed rectangular area.

The three spectral analysis regions on the NW rim were fitted with an absorbed *single power-law* model and an absorbed *srcut* model [15,16,28]. While applying the *power-law* model, as in the spectral analysis of the N region, N_H was fixed to 6.7 $\times$ 10^{21} cm^{-2}, and the other parameters were set free. While fitting the *srcut* model, a synchrotron origin was assumed for the hard X-ray emission observed from the SNR, and employed spectral index (α) and flux density values were assumed to be approximately 0.52 and 0.074 Jy at 1 GHz [29], respectively, while the galactic hydrogen column density parameters were set as free for the sources region-1 and region-2. In the previous studies of Vela Jr., α was approximately 0.3 in the NW region [30], and the flux density at 1 GHz was approximately 50 Jy from entire region of the SNR [31].

After spectral analysis of region-1 and region-2, they were excluded from emission region-3 (Figure 2) in order to characterize the whole nonthermal emission of the NW rim, taking into account the nearby emission of these X-ray peaks (Figure 2). All spectra were fitted in the 2.0–5.0 keV range in order to focus on the effective high-energy band from the emission. The best-fit parameters are shown in Tables 6 and 7 for BGD-1 and BGD-2 subtracted spectra, respectively. The BGD-2 subtracted ACIS-S spectrum is shown in Figure 4, which represents an example of the X-ray spectra of Vela Jr. as extracted from the NW rim. The spectra for each region, with two estimated background methods, have features similar to the spectrum shown in Figure 4.

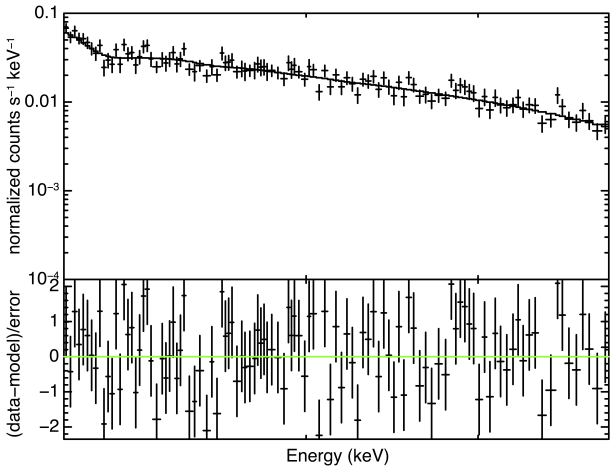


Figure 4. BGD-2 subtracted spectrum of the selected emission region-1 on the NW rim, fitted with an absorbed *power-law* model in the 2–5 keV energy band. The figure shows an example of the X-ray spectra of the NW region.

3. Results and discussion

In this paper, Vela Jr. was studied in the X-ray band using data from the *Chandra* Observatory. The nonthermal emission from the NW and N rims of the SNR were initially investigated using the selected emission regions; thus, the X-ray spectrum of each of the two rims was analyzed separately. Both rims have a power-law continuum spectrum for $E_x \geq 2.0$ keV, which can be also well fitted by the *srcut* model of XSPEC for the NW rim.

The best-fit parameters of the BGD-2 subtracted spectrum of the N rim was provided by an absorbed single *power-law* model with a χ^2 / d.o.f. value of approximately 1.07, with Γ of approximately 2.55. On the other hand, the best-fit parameters of the BGD-2 subtracted spectrum gave the values of a breaking energy of approximately 4.85 keV for Γ and approximately 2.37 for $E < E_{break}$, and Γ was approximately 0.15 for $E > E_{break}$ with a χ^2 / d.o.f. value of 1.02. An absorbed single *power-law* model gave a high χ^2 / d.o.f. value for this spectrum. Eventually, the photon index value of the BGD-2 subtracted spectrum is lower than the value of the BGD-1 subtracted spectrum.

Table 6. Best-fit parameters for BGD-1 subtracted spectrum of selected emission region on the north-western rim of Vela Jr.

Component	Parameter	Values		
		Source No. 1	Source No. 2	Source No. 3
power-law	N_H (10^{22} cm^{-2})	0.67 (fixed)	0.67 (fixed)	0.67 (fixed)
	Photon index	2.52 (2.64–2.40)	2.64 (2.78–2.50)	2.52 (2.60–2.44)
	norm (10^{-3} photons cm^{-2} s^{-1})	0.79 (0.90–0.69)	0.67 (0.76–0.57)	2.05 (2.23-1.88)
	χ^2/ d.o.f.	115.25 / 108	85.06 / 84	170.63 / 182
srcut	N_H (10^{22} cm^{-2})	0.98 (1.33-0.63)	0.92 (1.34–0.50)	0.67 (fixed)*
	Spectral index (α)**	0.52 (fixed)	0.52 (fixed)	0.52 (fixed)
	$\nu_{rolloff}$ (10^{16} Hz)	10.14 (10.64–9.65)	7.84 (8.27–7.42)	27.03 (27.73–26.34)
	norm (Jy at 1 GHz)**	0.074 (fixed)	0.074 (fixed)	0.074 (fixed)
	χ^2/ d.o.f.	115.95 / 108	85.98 / 84	196.59 / 193

*[26], **[29].

Table 7. Best-fit parameters for BGD-2 subtracted spectrum of selected emission region on the north-western rim of Vela Jr.

Component	Parameter	Values		
		Source No. 1	Source No. 2	Source No. 3
power-law	N_H (10^{22} cm^{-2})	0.67 (fixed)	0.67 (fixed)	0.67 (fixed)
	Photon index	2.42 (2.53–2.31)	2.53 (2.66–2.40)	2.37 (2.45–2.29)
	norm (10^{-3} photons cm^{-2} s^{-1})	0.77 (0.87–0.68)	0.64 (0.74–0.55)	2.02 (2.09–1.96)
	χ^2/ d.o.f.	115.99 / 108	85.17 / 84	167.78 / 182
srcut	N_H (10^{22} cm^{-2})	1.14 (1.47–0.82)	1.12 (1.51–0.73)	0.67 (fixed)*
	Spectral index (α)**	0.52 (fixed)	0.52 (fixed)	0.52 (fixed)
	$\nu_{rolloff}$ (10^{16} Hz)	11.12 (11.64–10.62)	8.51 (8.94–8.08)	33.32 (34.07–32.58)
	norm (Jy at 1 GHz)**	0.074 (fixed)	0.074 (fixed)	0.074 (fixed)
	χ^2/ d.o.f.	119.98 / 108	88.63 / 84	179.51 / 183

*[26], **[29].

On the other hand, for all the emission regions, with the best-fit parameters of the BGD-2 subtracted spectra of NW, the photon indices are lower than those of the BGD-1 subtracted one. This situation is opposite for the *srcut* model and the roll-off frequency (ν_{roll}), and it is slightly higher than the previous approach. Moreover, both situations gave acceptable reduced χ^2 values.

In summary, for both N and NW rim analysis, one can clearly see that the photon indices of the BGD-2 subtracted spectra of emission regions (Tables 5 and 7) are always lower than the ones in the classical background estimation method (Tables 4 and 6). Furthermore, while these results are compatible between each other, they are lower than the calculated Γ results in the literature. A similar situation is observed for the calculated roll-off frequencies in this study. Formally (i.e. based on reduced χ^2), the fits are acceptable for BGD-1 and BGD-2 subtracted spectra for both the NW and N rims, with significant difference of the best-fit photon index and roll-off frequency parameters for the two regions.

In the *Chandra* study of the NW rim, the roll-of frequency was approximately 4.3 $\times$ 10^{16} Hz according to the *srcut* spectra of the selected filaments. In the other *Chandra* study [29], ν_{roll} was approximately 15.80 $\times$ 10^{16} Hz, assuming a spectral index of approximately 0.52 for the selected emission regions and also that Vela

Jr. does not currently accelerate electrons to the "knee" energy of the cosmic ray spectrum. In this study, for both BGD-1 and BGD-2 subtracted spectra, the roll-off frequency was lower than these values (Tables 6 and 7) for the selected regions; only region-3 had higher values than these.

4. Conclusions

In this work, the results of spectral analysis of Vela Jr. based on *Chandra* observations are presented, and two regions of this remnant are studied. The conclusions can be summarized as follows:

1. The NW rim was studied as two separated filament-like structures and their surrounding environment. The N rim analysis was carried out with one emission region. The high-energy sections of the spectra of both rims are consistent with a *power-law* shape. Therefore, spectra were extracted from four regions that were sampled using the ACIS-S and ACIS-I arrays and were fit using a simple power-law, a *broken power-law*, and a synchrotron model *srcut*. Statistically acceptable fits were derived using each model by subtracting modeled and nonmodeled background spectra.

2. A precise background modeling affects the results of spectral analysis. For example, a reliable method might be effective in estimating the maximum energy of accelerated electrons ($E_{max,e}$), which is calculated from roll-off frequency, and a key parameter for understanding the spectrum of synchrotron emission. For this reason, two different background methods were employed (described in Section 2.2.1) to estimate the spectral parameters of Vela Jr. As already implied, statistically acceptable fits were derived. However, slight variations were seen in derived fit parameters of the photon indices and roll-off frequencies between modeled and nonmodeled background spectra. These variations possibly indicate the differences in how background estimation methods affect the analysis results.

References

[1] Koyama, K.; Petre, R.; Gotthelf, E. V.; Hwang, U.; Matsuura, M.; Ozaki, M.; Holt, S. S. *Nature* **1995**, *378*, 255-258.

[2] Koyama, K.; Kinugasa, K.; Matsuzaki, K.; Nishiuchi, M.; Sugizaki, M.; Torii, K.; Yamauchi, S.; Aschenbach, B. *Publ. Astron. Soc. Jpn.* **1997**, *49*, L7-L11.

[3] Nakamura, R.; Bamba, A.; Dotani, T.; Ishida, M.; Yamazaki, R.; Kohri, K. *Ap. J.* **2012**, *746*, 134-139.

[4] Slane, P.; Gaensler, B. M.; Dame, T. M.; Hughes, J. P.; Plucinsky, P. P.; Green, A. *Ap. J.* **1999**, *525*, 357-367.

[5] Slane, P.; Hughes, J. P.; Edgar; R. J.; Plucinsky, P. P.; Miyata, E.; Tsunemi, H.; Aschenbach, B. *Ap. J.* **2001**, *548*, 814-819.

[6] Vink, J.; Laming, J. M. *Ap. J.* **2003**, *584*, 758-769.

[7] Aschenbach, B. *Nature* **1998**, *396*, 141-142.

[8] Allen, G. E.; Chow, K.; DeLaney, T.; Filipovic, M. D.; Houck, J. C.; Pannuti, T. G.; Stage, M. D. *Astrophys. J.* **2015**, *798*, 82-94.

[9] Bamba, A.; Yamazaki, R.; Hiraga, J. S. *Ap. J.* **2005**, *632*, 229-240.

[10] Iyudin, A. F.; Aschenbach, B.; Becker W.; Dennerl, K.; Haberl, F. *Astron. Astrophys.* **2005**, *429*, 225-234.

[11] Uchiyama, H.; Nobukawa, M.; Tsuru, T.; Koyama, K. *Publ. Astron. Soc. Jpn.* **2013**, *65*, 61.

[12] Sato, T.; Koyama, K.; Takahashi, T.; Odaka, H.; Nakashima, S. *Publ. Astron. Soc. Jpn.* **2014**, *66*, 124-133.

[13] Katsuda, S.; Acero, F.; Tominaga, N.; Fukui, Y.; Hiraga, J. S.; Koyama, K.; Lee, S.; Mori, K.; Nagataki, S.; Ohira, N. et al. *Ap. J.* **2015**, *814*, 29-40.

[14] Bamba, A.; Fukazawa, Y.; Hiraga, J. S.; Hughes, J. P.; Katagiri, H.; Kokubun, M.; Koyama, K.; Miyata, E.; Mizuno, T.; Mori, K. et al. *Publ. Astron. Soc. Jpn.* **2008**, *60*, S153-S162.

[15] Reynolds, S. P. *Ap. J.* **1998**, *493*, 375-396.

[16] Reynolds, S. P.; Keohane, J. W. *Ap. J.* **1999**, *525*, 368-374.

[17] Bamba, A.; Yamazaki, R.; Ueno, M.; Koyama, K. *Ap. J.* **2003**, *589*, 827-837.

[18] Bamba, A.; Yamazaki, R.; Yoshida, T.; Terasawa, T.; Koyama, K. *Ap. J.* **2005**, *621*, 793-802.

[19] Smith R. K.; Brickhouse N. S.; Liedahl D. A.; Raymond J. C. *Ap. J.* **2001**, *556*, L91-L95.

[20] Foster A. R.; Ji L.; Smith R. K.; Brickhouse N. S. *Ap. J.* **2012**, *756*, 128-139.

[21] Krivonos, R.; Revnivtsev, M.; Churazov, E.; Sazonov, S.; Grebenev, S.; Sunyaev, R. *Astron. Astrophys.* **2007**, *463*, 957-967.

[22] Kushino A.; Ishisaki Y.; Morita U.; Yamasaki N. Y.; Ishida M.; Ohashi T.; Ueda Y. *Publ. Astron. Soc. Jpn.* **2002**, *54*, 327-352.

[23] Kalberla, P. M. W.; Burton, W. B.; Hartmann, D.; Arnal, E. M.; Bajaja, E.; Morras, R.; Pöppel, W. G. L. *Astron. Astrophys.* **2005**, *440*, 775-782.

[24] Bamba, A.; Terada, Y.; Hewitt, J.; Petre, R., Angelini, L.; Safi-Harb, S.; Zhou, P.; Bocchino, F.; Sawada, M. *Ap. J.* **2016**, *818*, 63.

[25] Yuasa, T.; Makishima, K.; Nakazawa, K. *Ap. J.* **2012**, *753*, 129.

[26] Hiraga, J. S.; Kobayashi, Y.; Tamagawa, T.; Hayato, A.; Bamba, A.; Terada, Y.; Petre, R.; Katagiri, H.; Tsunemi, H. *Publ. Astron. Soc. Jpn.* **2009**, *61*, 275-281.

[27] Wilms J.; Allen A.; McCray R. *Ap. J.* **2000**, *542*, 914-924.

[28] Hendrick, S. P.; Reynolds, S. P. *Ap. J.* **2001**, *559*, 903-908.

[29] Pannuti G. T.; Allen, G. E.; Filipovic, M. D.; De Horta, A.; Stupar, M.; Agrawal, R. *Ap. J.* **2010**, *721*,1492-1508.

[30] Combi, J. A.; Romero, G. E.; Benaglia, P. *Ap. J.* **1999b**, *519*, L177-L180.

[31] Duncan, A. R., Green, D. A. *Astron. Astrophys.* **2000**, *364*, 732-740.